Acta Crystallographica Section F
Structural Biology and Crystallization Communications
ISSN 1744-3091

Crystallization of the glycogen-binding domain of the AMP-activated protein kinase β subunit and preliminary X-ray analysis

Galina Polekhina,[a]* Susanne C. Feil,[a] Abhilasha Gupta,[a] Paul O'Donnell,[b] David Stapleton[a] and Michael W. Parker[a]

[a]St Vincent's Institute of Medical Research, 9 Princes Street, Fitzroy, Victoria 3065, Australia, and [b]Department of Biochemistry and Molecular Biology, The University of Melbourne, Parkville 3010, Australia

Correspondence e-mail: gpolekhina@svi.edu.au

Received 19 August 2004
Accepted 5 October 2004
Online 9 October 2004

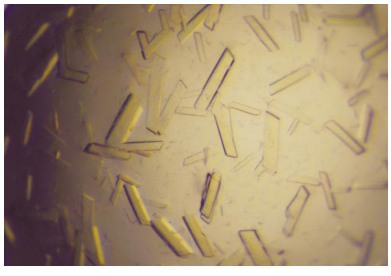

AMP-activated protein kinase (AMPK) is an intracellular energy sensor that regulates metabolism in response to energy demand and supply by adjusting the ATP-generating and ATP-consuming pathways. AMPK potentially plays a critical role in diabetes and obesity as it is known to be activated by metformin and rosiglitazone, drugs used for the treatment of type II diabetes. AMPK is a heterotrimer composed of a catalytic α subunit and two regulatory subunits, β and γ. Mutations in the γ subunit are known to cause glycogen accumulation, leading to cardiac arrhythmias. Recently, a functional glycogen-binding domain (GBD) has been identified in the β subunit. Here, the crystallization of GBD in the presence of β-cyclodextrin is reported together with preliminary X-ray data analysis allowing the determination of the structure by single isomorphous replacement and threefold averaging using in-house X-ray data collected from a selenomethionine-substituted protein.

1. Introduction

AMP-activated protein kinase (AMPK) coordinates energy metabolism in response to a variety of stimuli including exercise and adipocyte-derived hormones, resulting in tissue-specific changes to fatty-acid β-oxidation, glycolysis, glucose transport and food intake (reviewed in Kemp *et al.*, 1999; Hardie *et al.*, 2003; Carling, 2004). In this way, AMPK functions as a critical focal point for whole-body and cellular mechanisms maintaining energy homeostasis. AMPK has attracted widespread interest since the discovery that metformin, which is used to treat type II diabetes, could activate the enzyme (Fryer *et al.*, 2002). The importance of AMPK as a key regulator has been further highlighted by the discovery of mutations in the AMPK γ subunits in pigs that cause glycogen-storage disease (Milan *et al.*, 2000) as well as in humans that affect the electrical properties of the heart (Gollob *et al.*, 2002).

AMPK is an $\alpha\beta\gamma$ heterotrimer with multiple subunit isoforms encoded by seven genes ($\alpha1$, $\alpha2$, $\beta1$, $\beta2$, $\gamma1$, $\gamma2$, $\gamma3$) allowing up to 12 isoenzyme combinations, each with varying tissue and subcellular expression. AMPK requires the presence of all three subunits for activity and is activated through phosphorylation on the α catalytic subunit by LKB1, a serine/threonine kinase mutated in Peutz–Jeghers syndrome (Woods *et al.*, 2003). AMPK α contains a serine/threonine catalytic domain, an autoinhibitory domain and a subunit-binding domain. AMPK β is myristoylated at the N-terminus, phosphorylated at multiple sites and contains a glycogen-binding domain (GBD) that we and others have recently identified (Hudson *et al.*, 2003; Polekhina *et al.*, 2003). The γ subunit contains two pairs of CBS domains that have been found in a number of enzymes and have been shown to bind the AMPK allosteric activator AMP (Scott *et al.*, 2004).

Several lines of evidence that link AMPK to glycogen exist such as glycogen synthase and glycogen phosphorylase co-localizing and co-immunoprecipitating with AMPK and mutations in the AMPK γ subunit leading to glycogen-storage disease in pigs, mice and humans (Chen *et al.*, 1999; Milan *et al.*, 2000; Gollob *et al.*, 2002; Hudson *et al.*, 2003; Polekhina *et al.*, 2003). The identification of GBD thereby provides a molecular relationship between AMPK and glycogen.

AMPK GBD is related to the *N*-isoamylase domain found in glycogen-branching enzyme (Hudson *et al.*, 2003; Polekhina *et al.*,

2003). We have modelled GBD based on a structural alignment of several *N*-isoamylase domains of starch and glycogen-branching enzymes and predicted one carbohydrate-binding site on the surface of the domain (Polekhina *et al.*, 2003). The model is supported by mutational analysis. We now report the expression, purification and crystallization of GBD and its selenomethionine-substituted L105M mutant, as well as the preliminary structure determination by single isomorphous replacement and threefold averaging using in-house X-ray data.

2. Experimental procedures and results

2.1. Expression and purification

The cloning, expression and purification of the rat AMPK β1 subunit GBD (68–163) has been described previously (Polekhina *et al.*, 2003). Briefly, GBD was cloned into pProEX HT (Invitrogen) and expressed as a His-tag fusion protein in BL21 cells. Protein expression was induced with 1 m*M* IPTG for 3 h at 310 K when the cell density reached an OD_{600} of 0.6. GBD was purified on an Ni–agarose column and precipitated with 60% $(NH)_2SO_4$ for 30 min at 277 K. The protein pellet was resuspended in 50 m*M* Tris–HCl pH 8.5 and desalted by gel filtration. The His tag was cleaved by overnight digestion at room temperature with a His-tagged TEV protease (Invitrogen). The TEV protease, the cleaved His tag and any uncleaved material were removed by a second round of purification on an Ni–agarose column. GBD was further purified by S100 gel-filtration chromotography (Amersham Pharmacia) in 50 m*M* HEPES pH 7.0.

Our attempts to determine the structure either by molecular replacement using the GBD model or by isomorphous replacement were unsuccessful. We therefore decided to introduce selenomethionine. No natural methionine residues were present in the GBD amino-acid sequence. Based on the GBD model and the structural alignment of *N*-isoamylase domains, Leu105 was chosen to be replaced by methionine since it was part of the hydrophobic core and two out of three *N*-isoamylase domains contain methionine in an equivalent position, while the third has a leucine. Site-directed mutagenesis was performed according to the manufacturer's instructions (Stratagene). The template used was pProEX HT/GBD and the oligonucleotides used were 5′-TGGAGCAAATTGCCC **ATG**ACTAGAAGCCAAAAC-3′ for the sense strand and 5′-GTT-TTGGCTTCTAGT**CAT**GGGCAATTTGCTCCA-3′ for the anti-sense strand. The L105M mutation was confirmed by DNA sequencing. GBD L105M was transformed into Novagen 834 (DE3) cells. For expression, one colony was inoculated into 3 × 100 ml minimal media (Molecular Dimensions) containing 40 µg ml^{-1} methionine (Sigma) and incubated overnight at 310 K with shaking. The pellet washed with water was resuspended into 3 × 1 l minimal media (Molecular Dimensions) containing 40 µg ml^{-1} selenomethionine (Sigma) and incubated at 310 K with shaking until an OD_{600} of 0.6 was reached, at which point protein expression was induced by the addition of 1 m*M* IPTG for an additional 4 h at 310 K. The purification of SeMet-GBD L105M followed the same protocol as for wild-type GBD. The incorporation of SeMet was confirmed by MALDI mass spectrometry. The yields of wild-type and SeMet L105M GBD were 2 and 6.7 mg per litre of culture, respectively.

2.2. Crystallization

Prior to crystallization, the wild-type GBD and SeMet L105M GBD were concentrated to 14 mg ml^{-1} in 50 m*M* HEPES pH 7.0. All crystallization trials were performed at 295 K using the hanging-drop vapour-diffusion techinque. Initial screens with the wild-type GBD did not produce any crystals. Cyclodextrins have previously been used in structural studies of starch-binding and glycogen-binding proteins (Sorimachi *et al.*, 1997; Pinotsis *et al.*, 2003). We have also shown that β-cyclodextrin competes for binding to GBD with glycogen (Polekhina *et al.*, 2003). Since β-cyclodextrin is only slightly soluble in water, GBD was incubated with β-cyclodextrin powder on a rotating wheel at 277 K overnight. Excess β-cyclodextrin was removed by centrifugation. The GBD–β-cyclodextrin complex was then subjected to a variety of crystallization screens. The best crystals were grown when 2 µl GBD–β-cyclodextrin was mixed with an equal volume of reservoir solution containing 100 m*M* MES pH 7.0, 28–30%(*w*/*v*) PEG monomethyl ether 5000. Within a week, crystals of typical dimensions 0.1 × 0.1 × 0.3–0.4 mm appeared (Fig. 1*a*). Crystals of selenomethionine-substituted mutant GBD L105M were obtained under the same conditions but grew to larger size (0.2 × 0.2 × 0.6 mm) and had a tendency to produce a larger number of single crystals (Fig. 1*b*).

2.3. Preliminary X-ray analysis and structure determination

Diffraction data were collected at 100 K and recorded on a MAR 345 imaging-plate detector (MAR Research, Germany) using Cu $K\alpha$ radiation from an in-house Rigaku RU-200 rotating-anode X-ray generator. Crystals were either flash-frozen from the crystallization drop or transferred into 100 m*M* MES pH 7.0 and 32%(*w*/*v*) PEG monomethylether 5000, with larger crystals requiring a higher PEG percentage for successful freezing. GBD crystals diffract to 2 Å resolution in-house (Fig. 2) and belong to space group *P*1, with unit-cell parameters a = 43.7, b = 45.3, c = 50.6 Å, α = 72.0, β = 69.1, γ = 65.3°. The data were indexed and scaled with the *HKL* package (Otwinowski & Minor, 1997). Diffraction data statistics are

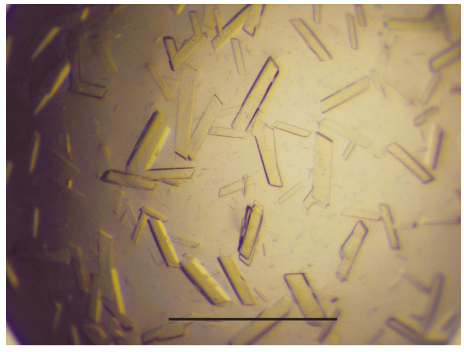

(*a*)

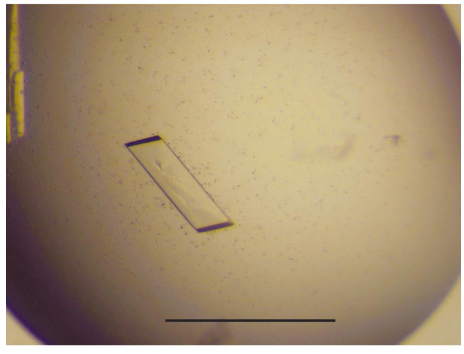

(*b*)

Figure 1
GBD crystals. (*a*) Wild type; (*b*) SeMet-substituted L105M mutant. The scale bar represents 1 mm.

Table 1
Data-collection and SIR phasing statistics.

Values in parentheses are for the highest resolution shell.

Data set	GBD	SeMet GBD L105M
Resolution (Å)	20–2.2 (2.3–2.2)	20–1.85 (1.89–1.85)
Unique reflections	15038 (1307)	25148 (1245)
Total observations	31525 (2413)	91210 (4071)
Redundancy	2.1 (1.85)	3.62 (3.27)
Completeness (%)	92.7 (80.1)	91.4 (67.0)
Mean $I/\sigma(I)$	28.0 (5.9)	29.11 (8.2)
$R_{\rm merge}$† (%)	3.0 (14.0)	4.1 (17.6)
Phasing statistics (20–3.0 Å)		
$R_{\rm iso}$‡ (%)	—	16.00
$R_{\rm Cullis}$§, acentric	—	0.66
Phasing power¶, acentric	—	1.89

† $R_{\rm merge} = \sum I - \langle I\rangle / \sum I$, where I is the intensity measurement for a given reflection and $\langle I\rangle$ is the average intensity for multiple measurements of this reflection. ‡ $R_{\rm iso} = \sum \big||F_{PH}| - |F_P|\big| / \sum |F_P|$, where F_{PH} and F_P are the derivative and native structure-factor amplitudes, respectively. § $R_{\rm Cullis} = \sum \big||F_{PH}| \pm |F_P|\big| - |F_H|\big| / \sum \big||F_{PH}| \pm |F_P|\big|$. ¶ Phasing power = root-mean-square of $(|F_H|/E)$, where F_H is the calculated heavy-atom structure-factor amplitude and E is the residual lack-of-closure error.

summarized in Table 1. Two or three molecules per unit cell are possible, corresponding to a calculated Matthews coefficient of 2.3 or 3.5 Å^3 Da^{-1} with 45 or 65% solvent content, respectively (Matthews, 1968). A self-rotation function did not resolve the ambiguity, as no significant peak corresponding to either twofold or threefold non-crystallographic symmetry was observed.

SeMet-substituted GBD L105M crystals were prepared in anticipation of an upcoming synchrotron trip. While waiting for the synchrotron trip, the quality of the crystals was assessed using the in-house X-ray source. We were able to easily determine the positions of three selenomethionines from the isomorphous difference Patterson maps calculated using in-house data from SeMet-substituted GBD L105M as a derivative and data from the wild-type GBD crystals as native (Fig. 3). The phasing statistics are shown in Table 1. The phases were improved by solvent flattening (*DM*; Collaborative Computational Project, Number 4, 1994). However, the obtained electron-density map was not unambiguously interpretable and the handedness could not be decided. As mentioned earlier, our attempts to determine the structure by molecular replacement using the GBD model were unsucessful. However, we have now established the positions of the three molecules in the unit cell as determined from the positions of the Se atoms. Using *AMoRe* (Navaza, 1994) and a GBD L105M model with the S atom of Met105 fixed at the origin, we calculated the rotation function at 15–4 Å resolution. The top rotation peak with an R factor of 53.2% and a correlation coefficient of 0.12 was taken as the first solution. All rotation peaks were then assigned a translation vector corresponding to the second SeMet position and were considered as a possible second solution. We then

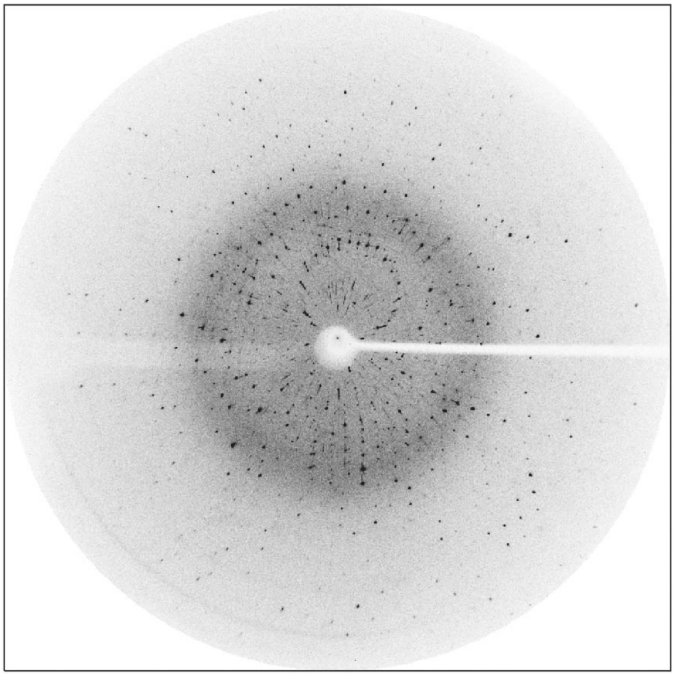

Figure 2
X-ray diffraction pattern from a crystal of SeMet-substituted GBD L105M.

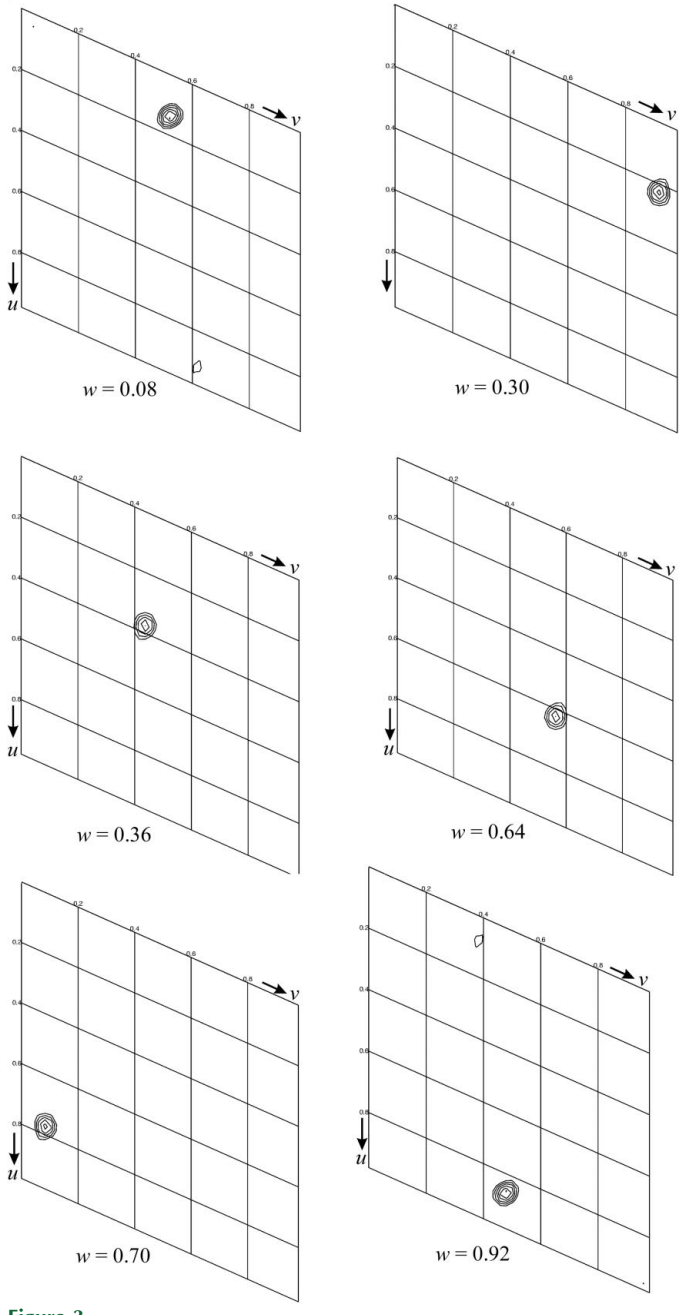

Figure 3
Six sections from the isomorphous difference Patterson map calculated at 20–4 Å resolution using in-house data from SeMet-substituted GBD L105M crystal as a derivative and in-house data from the wild-type GBD crystal. Contours above 3σ are shown in steps of 1σ.

performed rigid-body refinement using *AMoRe* at 15–4 Å resolution for each of the possible solution pairs. The best pair had an *R* factor of 50.7% and a correlation coefficient of 0.27 and identified the 47th rotation peak as a rotation solution corresponding to the second SeMet position. Again, all rotation solutions were assigned a translation vector according to the third SeMet position and each was considered as a possible third solution together with the best pair. After rigid-body refinement, the best solution triple gave an *R* factor of 49.3%, a correlation coefficient of 0.31 and identified the 12th rotation peak as a rotation solution for the third molecule. We also performed the calculations corresponding to the alternative enantiomorph, which resulted in an *R* factor of 50.7% and a correlation coefficient of 0.29 for the top solution triple. On the basis of these statistics we chose the former solution, in which two molecules are related by an approximate twofold symmetry ($\kappa = 162^\circ$) and the third molecule is related to either of the two by an improper symmetry, thus explaining why no self-rotation peak was found. Non-crystallographic symmetry matrices were derived from the molecular-replacement solution. Threefold averaging was then incorporated into the density modification in addition to solvent flattening performed using *DM* (Collaborative Computational Project, Number 4, 1994) at 20–3 Å resolution. The resulting electron density was easily interpretable. Refinement of the model is now in progress.

GP and DS are supported by NHMRC RD Wright Research Fellowships and MWP is a NHMRC Senior Principal Research Fellow. This work was also supported by a grant from the National Health and Medical Research Council of Australia (NHMRC) to MWP.

References

Carling, D. (2004). *Trends Biochem. Sci.* **29**, 18–24.
Chen, Z., Heierhorst, J., Mann, R. J., Mitchelhill, K. I., Michell, B. J., Witters, L. A., Lynch, G. S., Kemp, B. E. & Stapleton, D. (1999). *FEBS Lett.* **460**, 343–348.
Collaborative Computational Project, Number 4 (1994). *Acta Cryst.* D**50**, 760–763.
Fryer, L. G., Parbu-Patel, A. & Carling, D. (2002). *J. Biol. Chem.* **277**, 25226–25232.
Gollob, M. H., Green, M. S., Tang, A. S. & Roberts, R. (2002). *Curr. Opin. Cardiol.* **17**, 229–234.
Hardie, D. G., Scott, J. W., Pan, D. A. & Hudson, E. R. (2003). *FEBS Lett.* **546**, 113–120.
Hudson, E. R., Pan, D. A., James, J., Lucocq, J. M., Hawley, S. A., Green, K. A., Baba, O., Terashima, T. & Hardie, D. G. (2003). *Curr. Biol.* **13**, 861–866.
Kemp, B. E., Mitchenhill, K. I., Stapleton, D., Michell, B. J., Chen, Z.-P. & Witters, L. A. (1999). *Trends Biochem. Sci.* **24**, 22–25.
Matthews, B. W. (1968). *J. Mol. Biol.* **33**, 491–497.
Milan, D., Jeon, J. T., Looft, C., Amarger, V., Robic, A., Thelander, M., Rogel-Gaillard, C., Paul, S., Iannuccelli, N., Rask, L., Ronne, H., Lundstrom, K., Reinsch, N., Gellin, J., Kalm, E., Roy, P. L., Chardon, P. & Andersson, L. (2000). *Science*, **288**, 1248–1251.
Navaza, J. (1994). *Acta Cryst.* A**50**, 157–163.
Otwinowski, Z. & Minor, W. (1997). *Methods Enzymol.* **276**, 307–326.
Pinotsis, N., Leonidas, D. D., Chrysina, E. D., Oikonomakos, N. G. & Mavridis, I. M. (2003). *Protein Sci.* **12**, 1914–1924.
Polekhina, G., Gupta, A., Michell, B. J., van Denderen, B., Murthy, S., Feil, S. C., Jennings, I. G., Campbell, D. J., Witters, L. A., Parker, M. W., Kemp, B. E. & Stapleton, D. (2003). *Curr. Biol.* **13**, 867–871.
Scott, J. W., Hawley, S. A., Green, K. A., Anis, M., Stewart, G., Scullion, G. A., Norman, D. G. & Hardie, D. G. (2004). *J. Clin. Invest.* **113**, 274–284.
Sorimachi, K., Le Gal-Coeffet, M. F., Williamson, G., Archer, D. B. & Williamson, M. P. (1997). *Structure*, **5**, 647–661.
Woods, A., Johnstone, S. R., Dickerson, K., Leiper, F. C., Fryer, L. G., Neumann, D., Schlattner, U., Wallimann, T., Carlson, M. & Carling, D. (2003). *Curr. Biol.* **13**, 2004–2008.